Multilayer structure in SeAsGeSi-based OTS for high thermal stability and reliability enhancement

C. Laguna, M. Bernard, J. Garrione, N. Castellani, V. Meli, S. Martin, F. Aussenac, D. Rouchon, N. Rochat, E. Nolot, et al.

Multilayer Structure in SeAsGeSi-based OTS for High Thermal Stability and Reliability Enhancement

C. Laguna[1,2], M. Bernard[1], J. Garrione[1], N. Castellani[1], V. Meli[1], S. Martin[1], F. Aussenac[1], D. Rouchon[1], N. Rochat[1], E. Nolot[1], G. Bourgeois[1], M. C. Cyrille[1], L. Militaru[2], A. Souifi[3], F. Andrieu[1] and G. Navarro[1,*]
[1]CEA, LETI and Univ. Grenoble Alpes, F-38000 Grenoble, France
[2]Univ Lyon, INSA Lyon, ECL, CNRS, UCBL, CPE Lyon, INL, UMR5270, 69621 Villeurbanne, France
[3]Univ. de Lyon, Ampere-UMR 5005, INSA Lyon, 69621 Villeurbanne, France.

***Abstract*—In this paper, we present an innovative Multilayer SeAsGeSi-based Ovonic Threshold Switching (OTS) Selector targeting high reliability for Crossbar arrays. We compare our Multilayer (ML) OTS with SeAsGeSi-based bulk alloy (SAGS). We demonstrate the high thermal stability of the ML stack against the Back-End-of-Line (BEOL) thermal budget as well as the reduction of the device-to-device variability and reliable switching operations up to 300°C. We study by Raman and FTIR spectroscopy the integrity of the ML OTS material after an annealing of 3 hours at 400°C. SeAsGeSi Multilayer OTS delays crystallization mechanism along cycling. We finally report the successful co-integration of our ML with Phase-Change Memory technology.**

I. Introduction

Ovonic Threshold Switching (OTS) technology, based on amorphous chalcogenide materials, has been investigated in the last years as a reliable Back-End Selector solution because of its unique switching properties. OTS enables highly dense Resistive Non-Volatile Memory Crossbar arrays with agressive shrinkage of the single cell area down to $4F^2$. Therefore, OTS Selector becomes a key volatile device that combines the capability to provide at the same time a high current density when switched in the ON state for resistive memory programming, and an ultra-low leakage current when switched back to the OFF state. Indeed, Phase-Change Memory (PCM) and OTS Selectors have been successfully integrated in 3D-stackable 1S1R cell (i.e. one selector and one resistance) [1]–[3]. However, one of the main concerns is the devices thermal stability. Devices should undergo a Back-End-of-Line (BEOL) thermal budget and ensure reliable behaviour at high operating temperatures around 160°C-180°C forecasting the introduction in advanced embedded circuits like in edge AI applications. Recent works show the possibility to improve the thermal stability of OTS alloys [1, 4], nevertheless material study should always be coupled to the investigation of the final devices thermal stability after the initialization step (i.e. called "firing") that could lead to an important evolution of the active layer. AsSe-based OTS selectors have been investigated for their high resistivity (with respect to SbSe-based OTS) and for their switching voltage compatibility with OTS+PCM co-integration [1, 2]. However, AsSe-based OTS materials featuring the best high temperature stability performance are based on four or even more elements and their high complexity could lead to an intrinsic variability on their electrical parameters [4, 5]. In order to address such issue, we recently demonstrated that OTS Multilayer (ML) structure is an interesting method to decrease variability without affecting the main device characteristics [6, 7].

In this work, we investigate the benefit of ML structure in SeAsGeSi-based quaternary alloys to increase the material thermal stability of initialized (i.e. after firing) devices. The improved yield is verified by an enhanced endurance, a reduced variability of electrical parameters and a higher operating temperature. We gather Raman and FTIR spectroscopic studies on as-deposited and annealed OTS full-sheets for a thorough investigation of their structure and its evolution after annealing up to 400°C. The fabricated OTS devices are then characterized at high operating temperature up to 300°C and after a BEOL-like annealing of 3 hours at 400°C. Finally, we demonstrate for the first time a successful co-integration of ML OTS with PCM.

II. OTS Physico-Chemical Analyses

We deposited our materials using magnetron reactive sputtering from a SeAsGeSi (SAGS) single target. To achieve ML structure, we alternated the deposition of layers of SAGS and GeN, the latter obtained from a Ge target under constant N flow. Material samples were capped without air-break with 3.5 nm thick carbon layer to prevent surface oxidation. Annealing procedure was performed in a pre-heated chamber under N flow at a selected temperature and time.

In **Fig. 1**, we report the Raman spectra obtained for samples as-deposited and annealed at 400°C for 3 hours. As-deposited SAGS and ML exhibit the same three main features: As-Se, Si-Se and Ge-Se. The Ge-Se contribution decreases with annealing in SAGS while ML spectra are not strongly affected by annealing. SAGS spectrum shows an evolution after annealing, which could correspond to the starting of material segregation. As shown in our previous work on SbSe-based OTS [6], the ML structure delays structural changes related to crystallization process in OTS layers. Indeed, the introduction of GeN layers in SAGS increases the Ge-Se bonds with respect to As-Se and Si-Se because of interlayer interactions leading

This work was partially funded by European commission, French State and Auvergne-Rhône Alpes region through ECSEL-IA 101007321 project StorAIge and French Nano2022 program.
*Corresponding author. E-mail: gabriele.navarro@cea.fr (Gabriele Navarro)

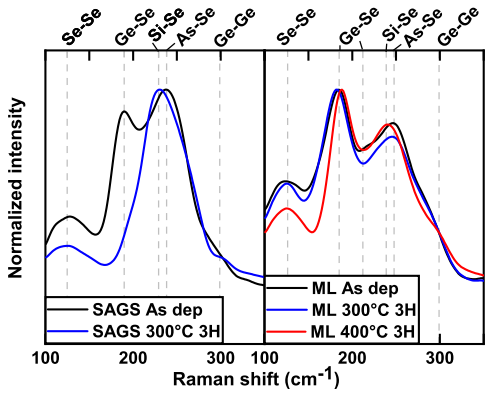

Fig. 1. Raman spectra of SAGS and ML as-deposited and after annealing for 3 hours at 300°C and 400°C. As-deposited, both materials show As-Se at 248 cm^{-1} [8, 9], Si-Se at 238 cm^{-1} [10] and Ge-Se features around 190 cm^{-1}(and 212 cm^{-1} for ML) [8, 11]–[13] with Ge-Ge shoulders at 300 cm^{-1}. Spectrum of SAGS annealed at 400°C is not reported because of the strong degradation of the sample after such annealing.

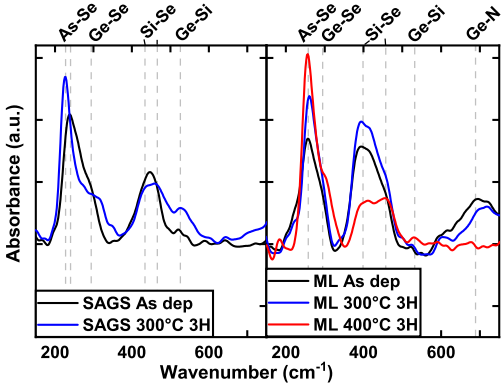

Fig. 2. FTIR spectra of SAGS and ML as-deposited and annealed at 300°C and 400°C during 3 hours. The feature at 230-300 cm^{-1} is a convolution of As-Se and Ge-Se vibrations [14, 15] and the one around 400 cm^{-1} is composed by at least two modes related to Si-Se vibrations [10]. In ML, a Ge-N feature is also observed at 690 cm^{-1} [16] at low temperature. Multiple features of difficult indexation are present around 830 cm^{-1} in ML after 400°C (not reported).

to Ge-Se bonds formation likely responsible for a higher layer stability.

In **Fig. 2**, we report the FTIR spectra for same samples. The spectra gather features linked to As-Se, Ge-Se, Si-Se, Ge-Si and Ge-N (only in ML) bonds vibrations. After annealing, we observe a thinning of the As-Se/Ge-Se convoluted feature, suggesting that the structural order is higher in annealed devices. Annealing modifies the shape of the double-mode Si-Se feature, favouring vibrations at higher frequencies. We observe Ge-N features in ML as-deposited and annealed at 300°C at 690 cm^{-1}. Despite the strong reduction of Ge-N features after annealing at 400°C we think that they should shift at higher frequencies (around 830 cm^{-1} [16]) due to their stabilization in Ge-poorer motifs. Unfortunately the analysis at such frequencies is perturbed by several other contributions in our samples preventing a correct indexation.

ML can undergo the annealing at 400°C without triggering crystallization nor segregation whereas bulk SAGS layer starts important structural changes. The increase of Ge-Se and addition of Ge-N features in ML delay crystallization phenomena and preserve the amorphous nature integrity of the OTS layer.

III. OTS Devices Electrical Characterization

We integrated SAGS and ML layers in analytical OTS single devices based on a tungsten bottom electrode with a diameter of 300 nm. A thin carbon layer is inserted between the OTS and the titanium nitride top electrode to prevent Ti diffusion within the chalcogenide layer. When not differently specified, data are obtained using AC measurements (i.e. pulsed voltage/current) on populations of 30 devices.

A. High operating temperature effects

In this section, we compare the electrical parameters of SAGS and ML up to an operating temperature of 300°C to evaluate their functionality in high temperature environment.

In order to evaluate the change of the conduction properties in the studied materials after firing, we performed DC current-vs-voltage measurements (IV chracteristics) at several temperatures in the sub-threshold regime before (virgin) and after firing (initialized). From the conducitivy dependency on the temperature, we interpolated the effective activation energy (E_m) for each voltage as reported in **Fig. 3** and compatibly with model reported in [17]. The extraction of the real activation energy (E_a) reveals that ML exhibits always a higher E_a with respect to SAGS (i.e. higher energy gap). The presence of additional Ge-Se features and the introduction of GeN [16], highlighted in material analyses, likely contribute to the increase of the energy gap in ML. Initialization is a process responsible of the creation of a channel in the OTS that likely has a different structural organization (and even composition) with respect to the virgin device. This is why the thermal stability of as-deposited layers could significantly differ from the one after firing.

We evaluated the functionality of the devices applying AC pulses inducing ON current in mA range. The initialization voltage (V_{fire}) and the threshold voltage (V_{th}) decrease when the operating temperature increase as shown in **Fig. 4**. SAGS devices do not show functionality above 250°C. At the same time, the leakage current (I_{off}) increases with operating temperature as already observed in [4, 6]. The saturation voltage

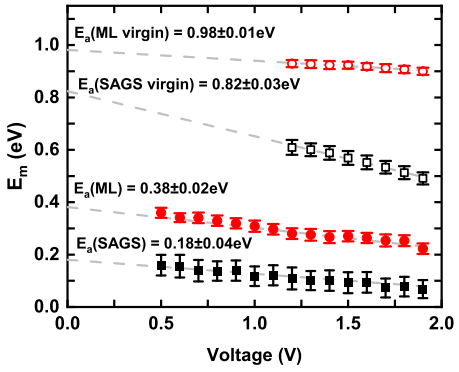

Fig. 3. Activation energy (E_a) extraction from E_m-vs-Voltage interpolations. E_m for each voltage is obtained by current vs temperature fitting (not reported) compatibly with [17] for virgin (before firing) and initialized devices (after firing). ML shows a higher activation energy (i.e. higher gap) with respect to SAGS before and after firing.

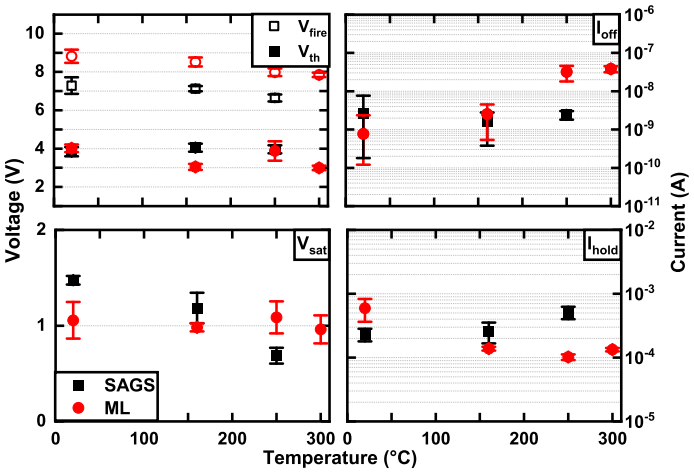

Fig. 4. Electrical parameters V_{fire}, V_{th}, V_{sat} and I_{hold} measured by AC protocols and I_{off} measured by DC voltage application (at $V_{th}/2$), from room temperature up to 250°C for SAGS and up to 300°C for ML. SAGS devices do not show functionality at 300°C.

(V_{sat}), calculated as the voltage drop on the devices at zero current extrapolated from ON current-vs-voltage characteristics, is stable in temperature for ML devices while it decreases in SAGS. We suggest that, considering the impact of annealing on SAGS reported in Fig. 1 and Fig. 2, the active material should evolve at 250°C. This leads to a reduction of the saturation voltage and an increase of the holding current (i.e. I_{hold}, the current needed to maintain the OTS in its ON state). On the contrary, the decrease of I_{hold} at high temperature in ML is compatible with the temperature activated ON conduction in the device (i.e. less current required to achieve the same temperature in the material to sustain the conduction in the ON state).

SAGS and ML show a high compatibility in terms of electrical parameters. However, ML OTS allows functionality up to higher temperatures: the addition of GeN layers in ML delays crystallization phenomena without degrading devices electrical properties and increases the activation energy of the conduction (i.e. higher energy gap).

B. BEOL thermal budget effects

In this section, we study the influence of a thermal budget on the devices electrical parameters, V_{th} drift and cycling capabilities. Devices were annealed in a pre-heated chamber at 400°C during 3 hours and slowly cooled within the chamber. Such high thermal budget can be assimilated to a BEOL thermal budget that the devices should overcome during a complete fabrication process. In the following, we will address as *As-fab* the initialized (after firing) devices after fabrication and as *400°C 3H* the initialized devices after annealing. As reported in **Fig. 5**, the annealing has similar effects as the ones observed at high operating temperatures. The structural evolution (i.e. relaxation) and the formation of stable features in the two materials lead to similar trends. Thus, the presence of GeN layers in ML does not affect the switching capabilities of SAGS-based chalcogenide glass even after annealing.

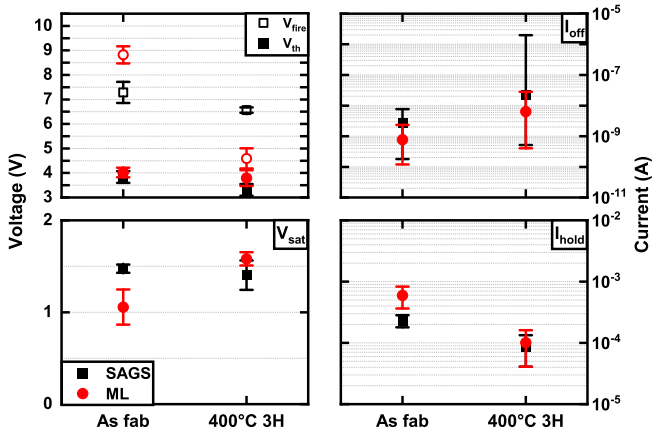

Fig. 5. Electrical parameters measured in AC (at the exception of I_{off} measured in DC) on devices as-fabricated and annealed for 3 hours at 400°C. The close electrical behavior of ML and SAGS, is likely related to the same features (i.e. AsSe) responsible for the switching mechanism in both materials.

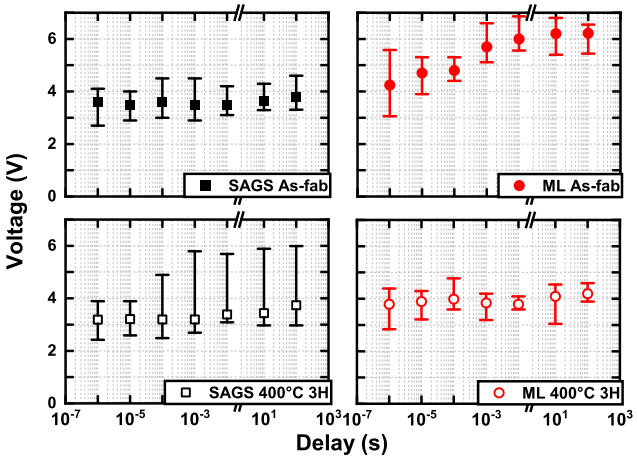

Fig. 6. V_{th} drift measured on as-fabricated and annealed devices. The defects related to Ge-Ge bonds owning to GeN layer in ML, present in *As-fab* devices, relax in time causing an important drift. After annealing, SAGS exhibits a median low drift affected by a 3 V spread while ML shows lower drift (with respect to *As-fab*) and low variability.

In **Fig. 6**, we report the V_{th} drift (i.e. the relaxation-induced changes after a given delay on the threshold voltage) in ML and SAGS devices as-fabricated and after annealing. Considering SAGS devices, the drift is low before annealing but after 3 hours at 400°C, device-to-device variability increases due to material degradation leading to a high drift in some devices. As-fabricated ML shows a high increase of V_{th} of about 2 V after 100 s from programming pulse, likely due to the presence of highly defective Ge-Ge bonds in GeN layers, which tend to relax after pulse application, as reported in [18]. Annealing, as observed in physico-chemical analyses, leads to the formation of stable GeN features and the increase of Ge-Se bonds, therefore to a reduction of Ge-Ge bonds in the system and a reduced drift in the device. Indeed, after annealing ML exhibits a reduced drift and low device-to-device variability.

Fig. 7 reports the maximum cycles number reached by SAGS and ML as-fabricated and after annealing together with the evolution of V_{th} along cycling on long and short time

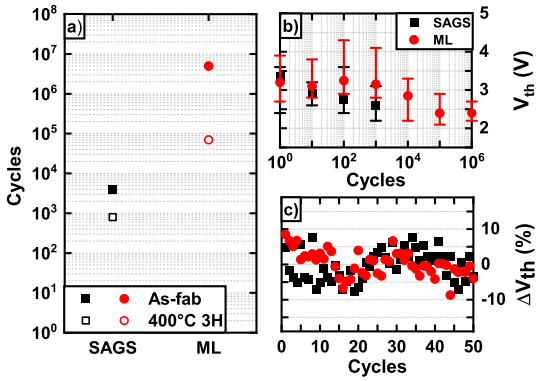

Fig. 7. a) Maximum cycles number reached preserving a selectivity between I_{on} and I_{off} of at least 10^3 in as-fabricated and annealed devices. The ML structure delays crystallization, enabling a higher endurance, however the annealing reduces cycling capabilities of both materials. **b)** V_{th} measured along cycling on as-fabricated devices. SAGS shows a V_{th} decrease since the first cycles while ML reaches 1000 cycles before showing a similar behavior. **c)** Cycle-to-cycle V_{th} variability during first 50 cycles: very low variation in the range of sensitivity used (about 0.2 V).

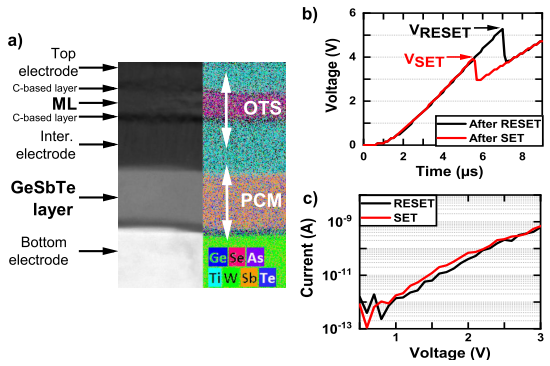

Fig. 8. a). TEM and EDX analyses of our ML OTS+PCM. **b)** V_{SET} and V_{RESET} switching voltages read by a voltage ramp applied on the OTS+PCM cell, after SET and RESET operations respectively. The reading window is higher than 1 V. **c)** Sub-threshold IV characteristics after SET and RESET pulses. A low leakage below 0.1 nA is ensured at half reading voltage (i.e. $(V_{SET}+V_{RESET})/2 \sim$ 2.2 V).

scales for as-fabricated devices. The degradation of SAGS material begins within the first cycles. On the contrary the structure of ML delays crystallization preserving the switching capability for a higher number of cycles. As-fabricated ML devices reach 10^6 cycles with a V_{th} decrease of 0.6 V that begins after the first 1000 cycles. To be noticed that ON current is kept at high values of about 1 mA during endurance tests. The structural evolution observed after annealing, seems to induce a higher sensitivity of the layer to ON current, being the endurance reduced of about 10 times. Cycle-to-cycle variability evaluated on first 50 cycles show a compatible results between the two materials.

ML OTS presents a lower device-to-device variability with respect to SAGS after BEOL-like thermal budget. Endurance capability is also enhanced in ML of at least 2 orders of magnitude.

C. Multilayer OTS and PCM co-integration

We successfully co-integrated ML OTS with PCM based on $Ge_2Sb_2Te_5$. In **Fig. 8**, we observe a reading window of more than 1 V between V_{SET} and V_{RESET} (respectively the switching voltages of the device when the PCM is programmed in SET and RESET state). Leakage current is kept below 0.1 nA at half of the reading voltage.

IV. Conclusions

We investigated Multilayer structure in SAGS-based OTS Back-End selectors to enhance thermal stability against BE-OL-like thermal budget of 3 hours at 400°C and improve switching reliability. We have demonstrated that ML OTS enables functionality at high operating temperatures up to 300°C, higher endurance and lower device-to-device variability. Finally, we provide demonstration of successful co-integration of ML OTS with PCM.

References

[1] H.Y. Cheng et al., "Si incorporation into AsSeGe chalcogenides for high thermal stability, high endurance and extremely low Vth drift 3D stackable cross-point memory", *in Proc. VLSI 2020*, pp. 1-2, 2020.

[2] D.C. Kau, "The pursuit of atomistic switching and cross point memory", *in Proc. VLSI-TSA 2021*, pp. 1-2, 2021.

[3] G. Navarro et al., "Innovative PCM+OTS device with high sub-threshold nonlinearity for non-switching reading operations and higher endurance performance", *in Proc. VLSI 2017*, pp. 1-2, 2017.

[4] D. Garbin et al., "Composition Optimization and Device Understanding of Si-Ge- As-Te Ovonic Threshold Switch Selector with Excellent Endurance", *in Proc. IEDM 2019*, pp. 35.1.1-35.1.4, 2019.

[5] H.Y. Cheng et al., "Optimizing AsSeGe chalcogenides by dopants for extremely low Ioff, high endurance and low Vth drift 3D crosspoint memory", *in Proc. IEDM 2021*, pp. 28.6.1-28.6.4, 2021.

[6] C. Laguna et al., "Multilayer OTS Selectors Engineering for High Temperature Stability, Scalability and High Endurance", *in Proc. IMW 2021*, pp. 1-4, 2021.

[7] S. Zhang et al., "A symmetric multilayer gese/gesesbte ovonic threshold switching selector with improved endurance and stability", *in Proc. ICTA 2021*, pp. 45-46, 2021.

[8] Y. Gan et al., "Analysis of Raman Spectra of GeAsSe Glass Using Different Peak-fitting Method", *in Proc. SPIE 2014*, vol. 9446, 2014.

[9] C.M. Schwarz et al., "Processing and fabrication of micro-structures by multiphoton lithography in germanium-doped arsenic selenide", *Opt. Mater. Express*, vol. 8, no. 7, pp.1902-1915, 2018.

[10] M. Tenhover et al., "Vibrational studies of crystalline and glassy $SiSe_2$", *Solid State Communications*, vol. 51, no. 7, pp. 455-459, 1984.

[11] C. Zha et al., "Optical properties and structural correlations of GeAsSe chalcogenide glasses", *J Mater Sci: Mater Electron*, vol. 18, pp. 389-392, 2007.

[12] P. Němec et al., "Structure and properties of the pure and Pr3+-doped $Ge_{25}Ga_5Se_{70}$ and $Ge_{30}Ga_5Se_{65}$ glasses", *J. Non-Cryst. Solids*, vol. 270, no. 1, pp. 137-146, 2000.

[13] M. Olivier et al., "Structure, nonlinear properties, and photosensitivity of $(GeSe_2)_{100-x}(Sb_2Se_3)_x$ glasses", *Opt. Express*, vol. 4(3), pp. 252-540, 2014.

[14] P. Khan et al., "Investigation of Temperature Dependent Optical Modes in $Ge_xAs_{35-x}Se_{65}$ Thin Films: Structure Specific Raman, FIR and Optical Absorption Spectroscopy", *Thin Solid Films*, vol. 621, pp. 76-83, 2017.

[15] M. Munzar et al., "Far-infrared spectra and bonding arrangement in Ge–As–S–Se glasses", *J. Phys. Chem. Solid.*, vol. 61, no. 10, pp. 1647-1652, 2000.

[16] I. Chambouleyron et al., "Nitrogen in germanium", *J. Appl. Phys.*, vol. 84, no. 1, pp. 1-30, 1998.

[17] D. Ielmini et al., "Analytical model for subthreshold conduction and threshold switching in chalcogenide-based memory devices", *J. Appl. Phys.*, vol. 102, no. 054517, pp.1-13, 2007.

[18] S. Clima et al., "Ovonic Threshold-Switching GexSey Chalcogenide Materials: Stoichiometry, Trap Nature, and Material Relaxation from First Principles", *Phys. Status Solidi RRL*, vol. 14, pp. 1900672, 2020.